New insight into calcium tantalate nanocomposite photocatalysts for overall water splitting and reforming of alcohols and biomass derivatives

Ping Wang, Philipp Weide, Martin Muhler, Roland Marschall, and Michael Wark

Citation: APL Materials **3**, 104412 (2015); doi: 10.1063/1.4928288
View online: http://dx.doi.org/10.1063/1.4928288
View Table of Contents: http://scitation.aip.org/content/aip/journal/aplmater/3/10?ver=pdfcov
Published by the AIP Publishing

New insight into calcium tantalate nanocomposite photocatalysts for overall water splitting and reforming of alcohols and biomass derivatives

Ping Wang,[1,a] Philipp Weide,[1] Martin Muhler,[1] Roland Marschall,[1,2] and Michael Wark[1,3,b]

[1]*Laboratory for Industrial Chemistry, Ruhr-University Bochum, Universitaetsstrasse 150, 44801 Bochum, Germany*

[2]*Institute of Physical Chemistry, Justus-Liebig-University Giessen, Heinrich-Buff-Ring 58, 35392 Giessen, Germany*

[3]*Institute of Chemistry, Technical Chemistry, Carl von Ossietzky University Oldenburg, Carl-von-Ossietzky-Str. 9-11, 26129 Oldenburg, Germany*

(Received 15 May 2015; accepted 28 July 2015; published online 7 August 2015)

The photocatalytic properties of different calcium tantalate nanocomposite photocatalysts with optimized phase composition were studied without the addition of any co-catalysts in the photoreforming of different alcohols including the biomass conversion by-product glycerol, as well as after modification with double-layered NiO_x (Ni/NiO) co-catalyst in overall water splitting (OWS). Nanocomposite photocatalyst consisting of cubic α-$CaTa_2O_6$/orthorhombic β-$CaTa_2O_6$ coexisting phases always possesses the highest photocatalytic performance. For overall water splitting, a loading of 0.5 wt. % NiO_x exhibits the best activities with stable stoichiometric H_2 and O_2 evolution rates. [http://dx.doi.org/10.1063/1.4928288]

In the past few decades, photocatalytic water splitting into H_2 and O_2 under solar radiation has attracted considerable attention as a potential way to renewable hydrogen fuel using semiconductor-based photocatalysts.[1] Up to now, although a number of single and multi-component semiconductors have been reported to be photocatalytically active for this reaction,[2–5] the energy conversion efficiency of semiconductor photocatalysts is still too low to meet the needs of industrial applications and, as a result, the search for efficient photocatalytic systems is continuously in progress.

A series of highly efficient calcium tantalate nanocomposite photocatalysts obtained by adjusting the precursors of Ta/Ca ratios in molten salt assisted syntheses was reported in our previous work,[6] structurally and optically characterized and tested for photocatalytic hydrogen formation from methanolic solutions under UV irradiation. The most active nanocomposites were formed with the initial precursor ratios of Ta/Ca of 1.2, 1.6, and 1.8, respectively. In all these nanocomposites, at least two different calcium tantalate phases are present to high amounts, i.e., cubic α-$CaTa_2O_6$ and hexagonal $Ca_2Ta_2O_7$ in the nanocomposite from Ta/Ca ratio of 1.2; cubic $CaTa_2O_6$, hexagonal $Ca_2Ta_2O_7$, and orthorhombic β-$CaTa_2O_6$ in the nanocomposite from Ta/Ca of 1.6; and cubic α-$CaTa_2O_6$ and orthorhombic β-$CaTa_2O_6$ in the nanocomposite from Ta/Ca of 1.8. The requirement of strong contributions of at least two phases demonstrates a synergistic effect concerning the charge separation by the coexisting phases. The proposed photoinduced electron-transfer pathways among the conduction band edges of these phase components via the interface junctions are the

[a]Present address: School of Energy and Chemical Engineering, Ulsan National Institute of Science and Technology, 50 UNIST-gil, Ulsan 689-798, South Korea.

[b]Author to whom correspondence should be addressed. Electronic mail: michael.wark@uni-oldenburg.de. Telephone: +49 441 798 3675. Fax: +49 441 798 3330.

following: The electrons on the surface of $Ca_2Ta_2O_7$ particles with the most negative conduction band potential can easily transfer to α- and β-$CaTa_2O_6$ particles, respectively, and similarly electron transfer from β-$CaTa_2O_6$ to α-$CaTa_2O_6$ is possible. Details to that can be found in Ref. 6.

The resulting lower recombination rates lead to improved photocatalytic activities. As an alternative strategy for effective enhancement via charge carrier separation, the rational fabrication of semiconductor composites comprising multicomponent or multiphase heterojunctions has attracted increasing attention.[7]

Therefore, one objective of the study presented here was to use our calcium tantalate nanocomposite photocatalysts with optimum phase-composition in a comparative study for reforming of different alcohols including the biomass conversion by-product glycerol, which is produced to large extent in bio-oil formation, as well as glucose as a carbohydrate representative in absence of any co-catalysts. The second focus in the study lies on OWS reaction for what the addition of a co-catalyst was found to be necessary. Since NiO_x is a cheap and effective co-catalyst for overall water splitting, the influence of NiO_x loading as co-catalysts for OWS is investigated in detail.

Calcium tantalate nanocomposite photocatalysts with optimum phase-composition were prepared by use of the "molten salt method" with initial Ta/Ca atomic ratios of 1.2, 1.6, and 1.8, respectively, as reported in our earlier work.[6] Briefly, the atomic ratios of Ta_2O_5 and Ca_2CO_3 precursors were ground with a mixture of 45:55 wt. % NaCl/KCl salts at a weight ratio of 1:2 and then calcined at 1123 K for 2 h in air using a corundum crucible. The resulting white powders were intensively washed with deionized water and dried at 353 K for 6 h. The samples with the initial Ta/Ca atomic ratios of 1.2, 1.6, and 1.8 are denoted as 1.2TC, 1.6TC, and 1.8TC, respectively.

For OWS, the as-synthesized optimum phase-composition composite photocatalysts were impregnated with different amounts of NiO_x as a function of Ni content (between 0.2 and 2.0 wt. %) according to a procedure described in detail elsewhere.[8,9] The as-synthesized powders were dispersed in a freshly prepared $Ni(NO_3)_2$ solution and heated under constant stirring until the water was completely evaporated. The resulting powder was dried at 353 K in air, followed by calcination at 473 K for 2 h, and further treated by reduction under H_2 flow at 573 K for 2 h and re-oxidation under O_2 flow at 473 K for 1 h. The NiO_x loaded calcium tantalate composite photocatalysts are generally denoted by NiO_x/TCs. For example, the 1.2TC composite photocatalyst with loading of 0.5 wt. % NiO_x co-catalysts is described in shorthand by 0.5 wt. % NiO_x/1.2TC.

Figure 1 shows the powder X-ray diffraction (XRD) patterns of 1.2TC (a), 1.6TC (b), and 1.8TC (c) composite photocatalysts: as-synthesized (pristine), loaded with 0.5 wt. % NiO_x, and recycled, after the photocatalytic reaction (with NiO_x), respectively. The crystalline phases were identified in reference to standard JCPDS cards. In good agreement with our previous results,[6] the XRD patterns

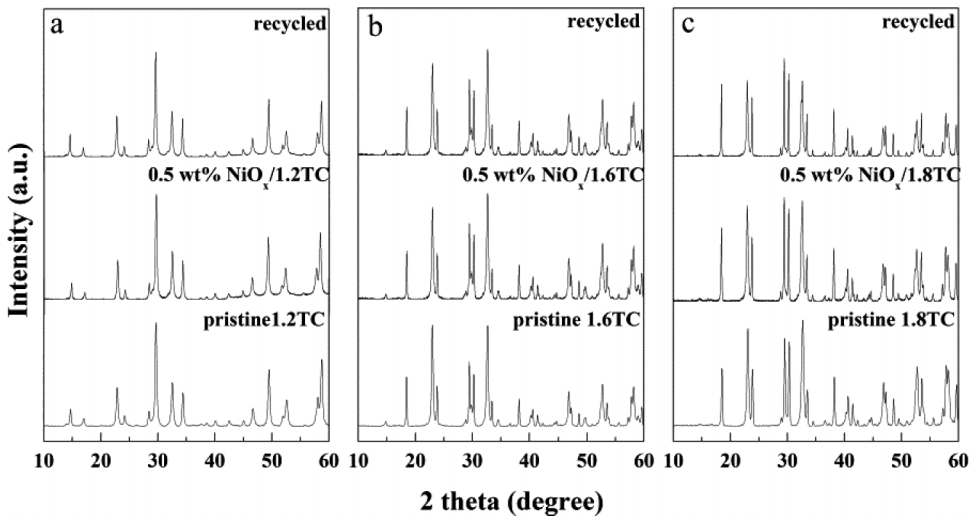

FIG. 1. XRD patterns of pristine TCs loaded with 0.5 wt. % NiO_x and recycled after photocatalytic water splitting: (a) 1.2TC, (b) 1.6TC, and (c) 1.8TC.

confirm that these samples were composed of cubic α-$CaTa_2O_6$ (JCPDS No. 36-0805)/hexagonal (hex.) $Ca_2Ta_2O_7$ (JCPDS No. 44-1008) phases, cubic $CaTa_2O_6$/hexagonal $Ca_2Ta_2O_7$/orthorhombic β-$CaTa_2O_6$ (JCPDS No. 39-1430) phases, and cubic α-$CaTa_2O_6$/orthorhombic β-$CaTa_2O_6$ phases, respectively. Moreover, no diffraction peaks of NiO_x were observed in the XRD patterns of 0.5 wt. % NiO_x loaded composite samples, due to low loading and the high dispersion, i.e., small size of less than about 2 nm, on the surface of the composite photocatalysts. After the photocatalytic reaction, no significant change was observed in the XRD patterns of the recycled NiO_x loaded samples, indicating that the composite photocatalysts are stable during the OWS reaction.

Figure 2 shows scanning electron microscopy (SEM) images (left) and energy-dispersive X-ray (EDX) spectra (right) of the composites loaded with 0.5 wt. % NiO_x: 1.2TC (a), 1.6TC (b), and 1.8TC (c), respectively. After loading NiO_x nanoparticles on the surface, no significant changes in morphology were observed by SEM in comparison to the images of pristine TCs shown in our earlier paper.[6] The 0.5 wt. % NiO_x/1.2TC sample is mainly composed of truncated hexagonal bipyramids of 0.2-0.5 μm in size, surrounded by a small portion of irregular particles. With the increasing of Ta/Ca ratio to 1.8TC an increasing number of elongated "truncated pyramid-like" shape rods with a length in the order of some few micrometers are formed, attached by a larger number of nanoparticles aggregates. This observed morphology evolution may be in favor for the formation of interface junctions between the β-$CaTa_2O_6$ and α-$CaTa_2O_6$ being in a more smooth contact.

As mentioned above, examination of these samples by XRD only revealed reflections attributed to calcium tantalate phases; however, the EDX analyses confirm the presence of nickel species. Furthermore, the identification of nickel species on the surface of the as-synthesized 0.5 wt. % NiO_x/TCs nanocomposites was performed by X-ray photoelectron spectroscopy (XPS) (Fig. 3).

As shown in Figure 3, the XP spectra of Ni 2p display a typical Ni^{2+} line shape with the Ni $2p_{3/2}$ and Ni $2p_{1/2}$ peaks located at 853.5 and 871.0 eV and characteristic satellite peaks at 860.5 and 879.0 eV, respectively.[10] The main Ni $2p_{3/2}$ peak at 853.5 eV is slightly shifted towards lower binding energy compared to pure NiO, which shows a band at 853.7 eV.[11] This is also consistent with data previously reported by Chiou *et al.*, who observed a similar shift of the Ni $2p_{3/2}$ peak

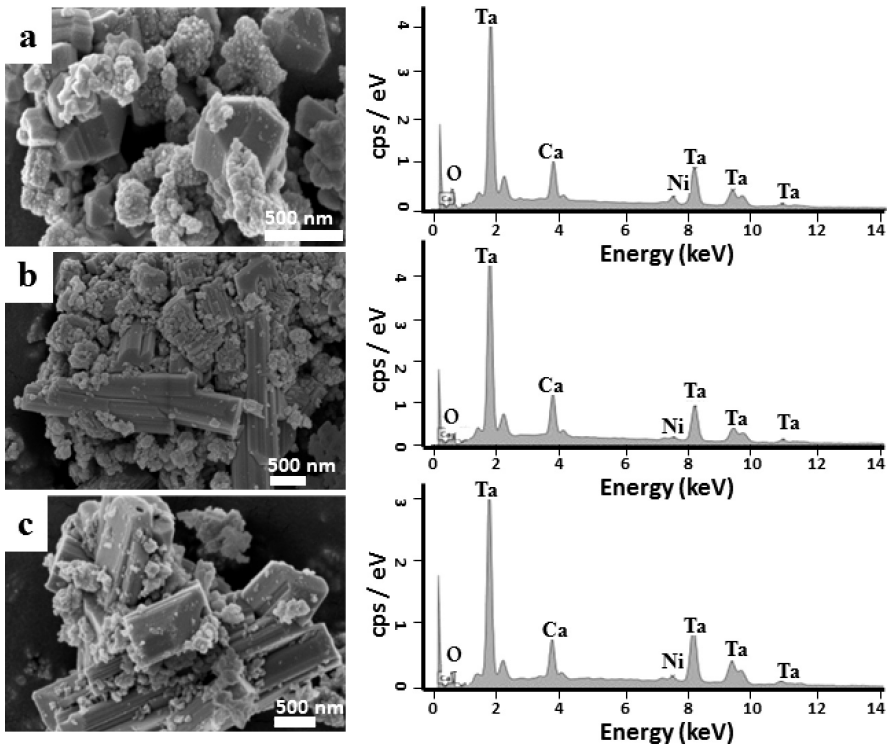

FIG. 2. SEM images (left) and EDX spectra (right) of the 0.5 wt. % NiO_x loaded calcium tantalate nanocomposites: (a) 1.2TC, (b) 1.6TC, and (c) 1.8TC.

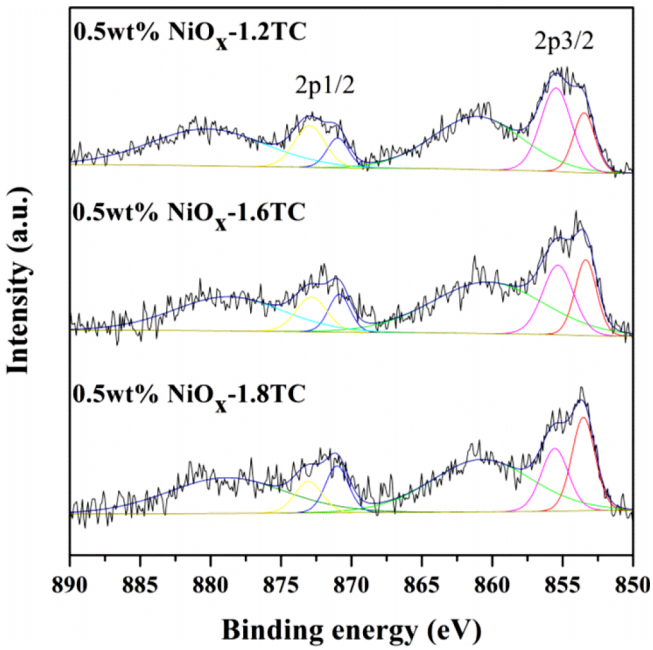

FIG. 3. Ni 2p XP spectra of as-synthesized 0.5 wt. % NiO_x/TCs nanocomposites.

after mild re-oxidation at 473 K in comparison to a fully oxidized or a reduced sample.[12] The shift is attributed to a combination of NiO and Ni, indicating a core-shell like structure with a thin layer of NiO covering the metal Ni core of the particles. The attempted deconvolution of the peak at 853.5 eV unfortunately gives no verified additional information; the different intensity ratios of the two sub-peaks might give some hint on altered thicknesses of Ni core and NiO shell, the 1.8TC sample showing a relatively larger peak intensity at lower binding energy indicating a larger Ni core, but a quantitative discussion would be too speculative. As a result of the complicate nanoparticle mixture in the study it is, however, very difficult to identify the morphology of the deposited NiO_x particles. But real-space transmission electron microscopy (TEM) observation of nanoscale double-layered NiO_x (Ni core/NiO shell) on well-dispersed $SrTiO_3$ nanoparticles had been initially performed by Osterloh *et al.*[13] And a clearly visible double-layer structure of NiO_x nanoparticles was further proven by our group from lattice-solved high-resolution TEM imaging on nanorod-shaped $Sr_2KTa_5O_{15}$ photocatalyst.[14] Based on the strong contrast between the nanorods and the NiO_x co-catalyst nanoparticles on top, a clear observation of different lattice fringes was possible. The formation of Ni metal at the surface of calcium tantalate nanocomposites results in the formation of Schottky contacts at the interface, which shift the calcium tantalate conduction band position to its maximum potential level and thus offer an opportunity to facilitate electron transport from the calcium tantalate to the NiO shell and, thus, effectively suppress the backward reaction between H_2 and O_2 as will be discussed below.[15]

Figure 4(a) shows the photocatalytic activity for OWS of composite photocatalysts with optimized phase compositions after loading with different amounts of NiO_x (between 0.2 and 2.0 wt. %). All the measurements were reproducibly conducted at least two or three times with different samples, and the same photocatalytic trend was obtained; deviations in the measured photocatalytic activities were below 5%. In general, all the catalysts show almost constant activities in subsequent runs. Without the deposition of NiO_x co-catalysts (i.e., 0 wt. % NiO_x), the composites exhibit low ability for OWS into stoichiometric amount of H_2 and O_2, probably due to the fast recombination of photogenerated electron-hole pairs but also the back-reaction of formed H_2 with O_2. With increasing amount of NiO_x as co-catalyst, their OWS activity is markedly enhanced reaching a maximum for a loading of 0.5 wt. % NiO_x. The results indicate that the NiO_x as co-catalysts not only greatly promotes the transfer of electrons enhancing the separation efficiency for photogenerated electron-hole pairs

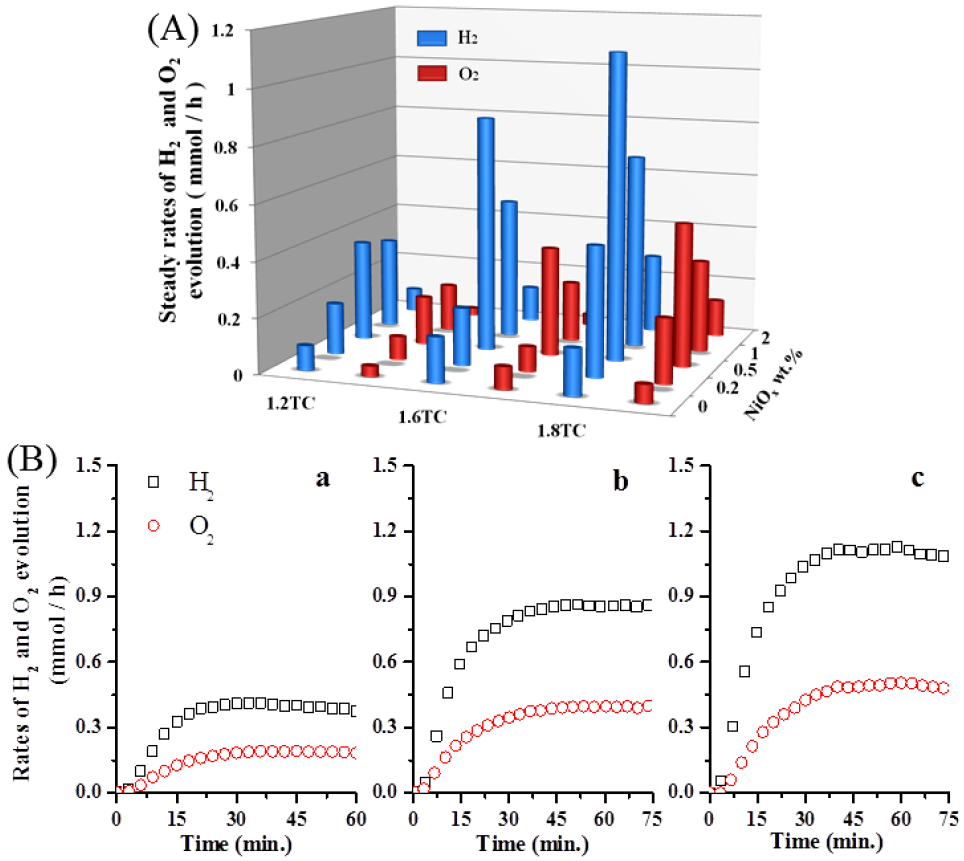

FIG. 4. (a) Effect of the NiO_x loading amount on photocatalytic activity of the composites for OWS into approximately stoichiometric amounts of H_2 and O_2. (b) Steady photocatalytic overall water splitting into stoichiometric amounts of H_2 and O_2 over these 0.5 wt. % NiO_x loaded composite photocatalysts (a) 1.2TC, (b) 1.6TC, and (c) 1.8TC. (Conditions: 500 W Hg mid-pressure immersion lamp, 0.5 g of photocatalyst, and 500 ml of water).

but also effectively suppresses the backward reaction between H_2 and O_2. This can be explained by cooperative effects between the formation of Schottky barriers at the metallic Ni/calcium tantalate contact regions and the existing heterojunctions between nanoparticles of the different phases in these calcium tantalate nanocomposites. However, NiO_x loading above 0.5 wt. % lowered the photocatalytic activity, because with higher loading the light masking by NiO particles might have a considerable detrimental effect on the photoreactivity. The number of surface sites responsive for light absorption is reduced if more NiO_x is present.

Figure 4(b) illustrates the simultaneous evolution of H_2 and O_2 over the optimum phase-composition composite photocatalysts with optimum loading of 0.5 wt. % NiO_x as a function of irradiation time. The production of hydrogen started with the lamp being turned on and the amount of the evolved gases increased linearly with UV irradiation time. After around 15 min, the steady evolution of H_2 and O_2 in an approximately stoichiometric amount can be observed, which can be attributed to the stabilization of the suspended particle systems and lamp radiation, and the saturation of water with evolved gases.[16] Figure 5 shows that for the photocatalyst composites with optimum phase-composition and optimum loading of 0.5 wt. % NiO_x, only small losses were observed in the typically performed three runs. Each run includes irradiation for 60-75 min. The results indicate a high stability of the photocatalytic OWS reaction, which is in accordance with the XRD results showing no degradation after the three runs.

Furthermore, the OWS activities of the as-synthesized calcium tantalate composite samples were compared with those reported in the literature (Table I). The single $CaTa_2O_6$ phase with perovskite-like orthorhombic (orth.) crystal structure, which was prepared by solid state reaction

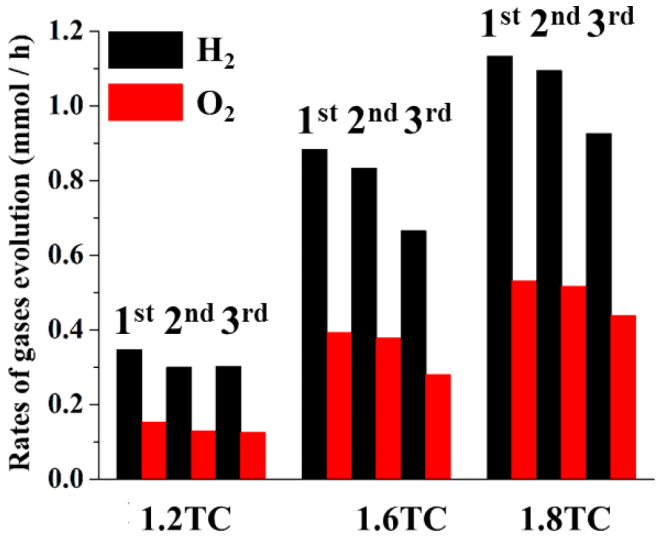

FIG. 5. Hydrogen and oxygen formation rates (taken after 60 min) in repeated photocatalytic OWS runs with the composites loaded with 0.5 wt. % NiO_x. (Conditions: 500 W Hg mid-pressure immersion lamp, 0.5 g of photocatalyst, and 500 ml of water).

method at 1450 K for 120 h,[17] shows low activity even after loading of 0.3 wt. % NiO as co-catalysts. Later, Ikeda *et al.*[18] claimed to have synthesized a single cubic pyrochlore $Ca_2Ta_2O_7$ phase using hydrothermal reaction method. However, the activity of 0.2 wt. % NiO loaded $Ca_2Ta_2O_7$ was still poor with the H_2/O_2 evolution rates of 0.17/0.08 mmol/h, while in the present work the as-synthesized calcium tantalate nanocomposites with optimum phase-composition obviously exhibited higher activity than these reported single phases. Undoubtedly, it benefited from the formation of the phase junctions and the improved charge transfer among the calcium tantalate composites. With optimum loading of 0.5 wt. % NiO_x on the 1.2TC, 1.6TC, 1.8TC composites, respectively, the significant enhancement in activity was found with the H_2/O_2 evolution rates of 0.39/0.19, 0.86/0.40, and 1.10/0.51 mmol/h, corresponding to the calculated photonic efficiencies of 0.135%, 0.297%, and 0.380%, respectively. For the NiO_x loaded composites at higher Ta/Ca ratio with the enhanced photocatalytic activity, the narrower band gap of the composites can be also considered to be a rational reason. Thus, more photons can be absorbed and consequently

TABLE I. Comparison of activities of calcium tantalate photocatalysts with different phase compositions for OWS.

Photocatalyst	Crystal structure	Mass (g)	Mercury lamp (W)	Co-catalyst/wt. %	Activity (mmol/h) H_2	Activity (mmol/h) O_2
$CaTa_2O_6$[17]	Orthorhombic	1.0	400	None	0.02	~0.01
				NiO/0.3	0.07	0.03
$Ca_2Ta_2O_7$[18]	Cubic	0.5	450	None	...	...
				NiO/0.2	0.17	0.08
1.2TC	Cubic/hexagonal[a]	0.5	500	None	0.09	0.04
				NiO_x/0.5	0.39	0.19
1.6TC	Cubic/hexagonal/orthorhombic[b]	0.5	500	None	0.16	0.07
				NiO_x/0.5	0.86	0.40
1.8TC	Cubic/orthorhombic[c]	0.5	500	None	0.17	0.06
				NiO_x/0.5	1.10	0.51

[a]Phase composed of cubic α-$CaTa_2O_6$ and hexagonal $Ca_2Ta_2O_7$.
[b]Phase composed of cubic $CaTa_2O_6$, hexagonal $Ca_2Ta_2O_7$ and orthorhombic β-$CaTa_2O_6$.
[c]Phase composed of cubic α-$CaTa_2O_6$ and orthorhombic β-$CaTa_2O_6$.

more electrons were excited to the conduction band, which is in good agreement with our previous work, where we discussed photocatalytic methanol reforming.[6] The results also demonstrate that the modification of double-layered NiO_x (Ni/NiO) as co-catalysts further facilitates electron transport and suppresses the backward reaction between H_2 and O_2.

OWS with NiO_x is already a quite green approach since it works without noble metals as co-catalyst but even better would be an efficient photocatalyst active without any co-catalysts. It was reported before that the calcium tantalate nanocomposites form hydrogen from methanol reforming without co-catalyst.[6] In order to confirm and generalize this finding, we tested our most active nanocomposite 1.8TC in pristine form for H_2 production by photocatalytic reforming of different alcohols, including methanol (MeOH), ethanol (EtOH), isopropyl alcohol (IPOH), and ethylene glycol (EG), as presented in Figure 6. Alcohols are known to show the current-doubling effect, and the reaction sequence is highly irreversible, and are hence greatly favorable for H_2 production.[19] The hydrogen production rates with the 1.8TC nanocomposite decreased in the following order: MeOH > EtOH > IPOH > EG, and by means of the standard potassium ferrioxalate actinometer as initially proposed by Hatchard and Parker,[20] their photonic efficiencies were calculated to be 3.45%, 2.52%, 2.28%, and 1.28%, respectively. The same order of photonic efficiencies was also observed over 1.2TC and 1.6TC nanocomposites (not shown). In summary, the use of MeOH always provides the best photocatalytic ability for H_2 production, due to its highest ability to donate electrons and to scavenge the valence band holes preventing photogenerated charge recombination. This agrees well with the reported order of hydrogen production efficiency over prototypical photocatalyst of Pt-loaded $KCa_2Nb_3O_{10}$.[21,22]

The use of by-products from biomass conversion for hydrogen production could be a useful intermediate step between the current fossil fuel energy structure and efficient water splitting.[23] The pioneering work of Kawai and Sakata in 1980 showed that hydrogen can be produced from carbohydrates over RuO_2/TiO_2/Pt photocatalyst under light irradiation.[24] Subsequently, they claimed that hydrogen can also be acquired from some other kinds of biomasses, such as cellulose, starch, dead insects, and waste materials.[25–27] In the present work, the 1.8TC nanocomposite photocatalyst (i.e., cubic α-$CaTa_2O_6$/orthorhombic β-$CaTa_2O_6$ phases) was thus further employed toward H_2 production by reforming of typical biomass derivatives. As shown in Figure 6, continuous H_2 evolution was observed from reforming of glycerol (GL, 50 ml), which is a by-product in biodiesel production formed in high amounts without existing market for such high quantities, and glucose (Glu, 0.1M) as a representative for carbohydrates. After irradiation for 180 min, the yield of evolved

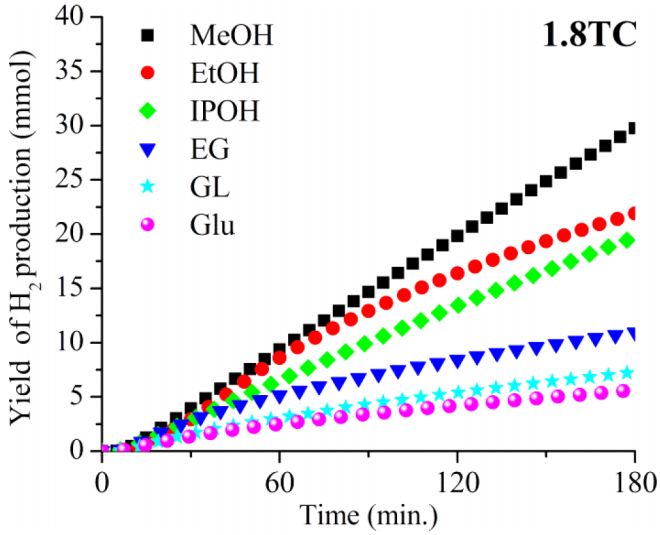

FIG. 6. Hydrogen evolution from aqueous solutions of different alcohols and biomass derivatives over 1.8TC nanocomposite photocatalyst without using any co-catalyst. (Conditions: 500 W Hg mid-pressure immersion lamp, 0.5 g of photocatalyst, 500 ml of water, and 50 ml of liquid alcohols or 0.1M of Glu).

H_2 was measured to be ca. 7.3 mmol and 5.6 mmol from aqueous GL and Glu solutions, respectively. Due to the electrochemical potential of glycerol the H_2 yield is lower than with the other alcohols, but a significant amount can be formed over time with only low deactivation. If compared to the photocatalytic activity of the 1.8 TC sample for H_2 production from OWS with the Ni/NiO co-catalyst (Fig. 4), the H_2 production from glycerol is almost doubled although no co-catalyst is present. This shows some potential; however, if cheap co-catalysts as the Ni/NiO system can be used, the OWS is more prospective.

In conclusion, the stoichiometric photocatalytic decomposition of water by calcium tantalate composites can be significantly enhanced by loading of NiO_x as co-catalysts. Nanocomposites consisting of cubic α-$CaTa_2O_6$ and β-orthorhombic $CaTa_2O_6$ phases loaded with 0.5 wt. % NiO_x showed the highest activity. We suggest that the enhanced photocatalytic activities can be attributed to the excellent catalytic properties of NiO and the cooperative effect between a Schottky barrier formed at the metallic Ni/calcium tantalate contact region with the interfacial heterostructure junctions in these calcium tantalate composites. This together promotes the interfacial charge separation and transfer and suppresses the backward reaction. Thus, the generation of the true "solar fuel" can be achieved by overall water splitting reaction, that is, photocatalytically split water into H_2 and O_2 in a stoichiometric ratio, thus converting the net solar energy into chemical energy. Without using any co-catalysts hydrogen from photocatalytic reforming of alcohols and biomass derivatives can also be achieved with these nanocomposites, the highest activity being observed for MeOH, the most effective electron donating species. These results reveal an efficient and noble metal-free photocatalytic reforming system for H_2 production. In case of glycerol, photocatalytic H_2 formation might help to improve the sustainability and economic benefit of the bio-refining industry. Moreover, the development of further advanced composite materials might be a route to cheaper, more efficient, and environmental-friendly photocatalysts for solar energy conversion.

We greatly appreciate Dr. T. Reinecke, Dr. R. Neuser, S. Schuenemann, and Dr. I. Sinev (all Ruhr-University Bochum, Germany) for XRD, SEM, actinometry measurements, and helpful discussions, respectively. R.M. gratefully acknowledges funding in the Emmy-Noether Program (No. MA 5392/3-1) of the Deutsche Forschungsgemeinschaft (DFG) and M.W. thanks the DFG for support under WA No. 1116/23. P.W. acknowledges scholarship support from the China Scholarship Council (CSC No. 2011614004).

[1] F. E. Osterloh, Chem. Mater. **20**, 35 (2008).
[2] S. T. Martin, A. T. Lee, and M. R. Hoffmann, Environ. Sci. Technol. **29**, 2567 (1995).
[3] A. Kudo and Y. Miseki, Chem. Soc. Rev. **38**, 253 (2009).
[4] X. B. Chen, S. H. Shen, L. J. Guo, and S. S. Mao, Chem. Rev. **110**, 6503 (2010).
[5] J. Soldat, R. Marschall, and M. Wark, Chem. Sci. **5**, 3746 (2014).
[6] P. Wang, P. Chen, A. Kostka, R. Marschall, and M. Wark, Chem. Mater. **25**, 4739 (2013).
[7] R. Marschall, Adv. Funct. Mater. **24**, 2421 (2014).
[8] K. Domen, A. Kudo, T. Onishi, N. Kosugi, and H. Kuroda, J. Phys. Chem. **90**, 292 (1986).
[9] X. Wang, Q. Xu, M. Li, S. Shen, X. Wang, Y. Wang, Z. Feng, J. Shi, H. Han, and C. Li, Angew. Chem., Int. Ed. **51**, 13089 (2012).
[10] C. P. Li, A. Proctor, and D. M. Hercules, Appl. Spectrosc. **38**, 880 (1984).
[11] M. C. Biesinger, B. P. Payne, L. W. M. Lau, A. Gerson, and R. S. C. Smart, Surf. Interface Anal. **41**, 324 (2009).
[12] Y. C. Chiou, U. Kumar, and J. C. S. Wu, Appl. Catal., A **357**, 73 (2009).
[13] T. K. Townsend, N. D. Browning, and F. E. Osterloh, ACS Nano **6**, 7420 (2012).
[14] P. Wang, L. Schwertmann, R. Marschall, and M. Wark, J. Mater. Chem. A. **2**, 8815 (2014).
[15] N. Zhang, S. Q. Liu, and Y. J. Xu, Nanoscale **4**, 2227 (2012).
[16] A. Galinska and J. Walendziewski, Energy Fuels **19**, 1143 (2005).
[17] H. Kato and A. Kudo, Chem. Lett. **28**, 1207 (1999).
[18] S. Ikeda, M. Fubuki, Y. K. Takahara, and M. Matsumura, Appl. Catal., A **300**, 186 (2006).
[19] Y. K. Kho, A. Iwase, W. Y. Teoh, L. Mädler, A. Kudo, and R. Amal, J. Phys. Chem. C **114**, 2821 (2010).
[20] C. Hatchard and C. A. Parker, Proc. R. Soc. A **235**, 518 (1956).
[21] A. Hameed and M. A. Gondal, J. Mol. Catal. A: Chem. **233**, 35 (2005).
[22] T. Kawai and T. Sakata, J. Chem. Soc., Chem. Commun. **1980**, 694.
[23] R. M. Navarro, M. C. Sanchez-Sanchez, M. C. Alvarez-Galvan, F. del Valle, and J. L. G. Fierro, Energy Environ. Sci. **2**, 35 (2009).
[24] T. Kawai and T. Sakata, Nature **286**, 474 (1980).
[25] T. Sakata and T. Kawai, New J. Chem. **5**, 279 (1981).
[26] T. Kawai and T. Sakata, Chem. Lett. **10**, 81 (1981).
[27] K. Hashimoto, T. Kawai, and T. Sakata, J. Phys. Chem. **88**, 4083 (1984).